Article

Engineering of the Conformational Dynamics of Lipase to Increase Enantioselectivity

Bin Yang, Hongjiang Wang, Wei Song, Xiulai Chen, Jia Liu, Qiuling Luo, and Liming Liu

ACS Catal., **Just Accepted Manuscript** • DOI: 10.1021/acscatal.7b02404 • Publication Date (Web): 27 Sep 2017

Engineering of the Conformational Dynamics of Lipase to Increase Enantioselectivity

*Bin Yang,[1,2] Hongjiang Wang,[1,2] Wei Song,[1,2] Xiulai Chen,[1,2] Jia Liu,[1,2] Qiuling Luo,[1,2] Liming Liu[1,2,]**

[1] State Key Laboratory of Food Science and Technology, Jiangnan University, Wuxi 214122, China

[2] Key Laboratory of Industrial Biotechnology, Ministry of Education, Jiangnan University, Wuxi 214122, China

* E-mail: mingll@jiangnan.edu.cn.

ABSTRACT: In order to increase the *R*-enantioselectivity of *Candida antarctica* lipase B (CALB) toward (*R*)-3-t-butyl-dimethyl-silyloxy glutaric acid methyl monoester at 30°C, we engineered CALB conformational dynamics. Based on structural analysis and molecular dynamics simulations, two key residues (D223 and A281) were identified, and three mutants (D223V, A281S, and D223V/A281S) were designed to decrease the conformational dynamics of the pocket and channel. Computational and experimental evaluations were performed for all mutants, with the D223V/A281S mutant exhibiting high *R*-enantioselectivity (>99.00%; increased from 8.00%) and high space-time yield (107.54 g L^{-1} d^{-1}; a 5.70-fold increase).

KEYWORDS: conformational dynamics, enantioselectivity, *Candida antarctica* lipase B, substrate pocket, substrate channel

INTRODUCTION

Recently, enzymes with high enantioselectivity have been widely used as biocatalysts to produce optically pure, valuable compounds.[1-6] However, in some cases, enzymes exhibit satisfactory enantioselectivity only at low temperatures (even down to –80°C), with decreasing enantioselectivity at higher temperatures.[7,8] Therefore, low-temperature methods have been applied to improve the enantioselectivity of some enzymes.[9-12] From a practical standpoint, although substantial efforts have been made to increase reaction rates at low temperatures, such as through the use of immobilized enzymes on porous ceramics,[9] the high costs and low yields associated with low temperatures remain limiting factors for industrial applications.[13] Some examples demonstrated the plausibility of maintaining satisfactory enzyme enantioselectivity at higher temperature through protein engineering[14]; however, simple and accurate strategies for protein engineering warrant further discussion.

Recently, there has been growing interest in the conformational dynamics of proteins, which play an important role in enzyme catalysis,[15-20] and engineering of enzyme conformational dynamics has become an effective strategy for protein evolution, achieving significant results in terms of relieving product inhibition[21-23] and for the rational design of enzymes.[24-26] Recent studies also indicated that protein conformational dynamics, which are crucial for ligand recognition and binding, might determine ligand-binding orientations, thereby assuming responsibility for selectivity.[19,27] Despite no direct reports on the relationship between enzyme conformational dynamics and enantioselectivity, engineering of enzyme conformational dynamics as a strategy is expected to guide improvements in enantioselectivity based on previous studies; however, the practical application of such a strategy for enzyme design remains a major challenge.

Candida antarctica lipase B (CALB; EC 3.1.1.3) is a member of the α/β-hydrolase family, possesses the catalytic triad S105-H224-D187, which lies between the two binding pockets (the acyl-binding pocket and the alcohol-binding pocket), and is widely used in both academic and industrial production.[28-35] The esterification of 3-t-butyl-dimethyl-silyloxy (TBDMSO) glutaric anhydride to (*R*)-3-TBDMSO glutaric acid methyl monoester, which is a multifunctional chiral building block of statins in the pharmaceutical industry, is catalyzed by CALB and was developed and optimized in a previous study (Scheme 1).[36] However, the CALB mutant, EF5, obtained by manipulating the substrate pocket exhibited high enantioselectivity toward (*R*)-1 [98.50%

enantiomeric excess (ee)] at 5°C and a low *R*-ee value of 8.00% at 30°C, which hindered industrial application. Here, we engineered CALB conformational dynamics to increase its enantioselectivity at 30°C. The most successful mutant, D223V/A281S (>99.00 ee at 30°C), was identified based on structural analysis and molecular dynamics (MD) simulations to decrease the conformational dynamics of the pocket and channel, thereby increasing enantioselectivity.

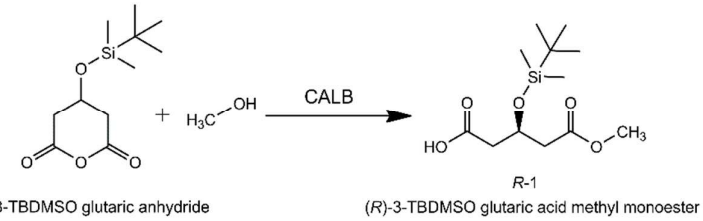

Scheme 1 The esterification scheme catalyzed by CALB.

RESULTS AND DISCUSSION

Effect of Temperature on the *R*-enantioselectivity of the EF5 Mutant

In our previous study, we obtained a CALB mutant, EF5.[36,37] Catalysis by the mutant EF5 showed an ee value and yield for (*R*)-3-TBDMSO glutaric acid methyl monoester of 98.50% and 13.20%, respectively, at 5°C. As shown in Figure 1A, increasing the temperature (from 5°C to 30°C) reduced EF5 *R*-enantioselectivity from 98.50% to 8.00% and, conversely, increased the yield from 13.20% to 80%. Furthermore, we investigated and compared the effect of temperature on the initial formation rates of the *R*- and *S*-enantiomers (Figure 1B), finding that the initial formation rates of the *R*- and *S*-enantiomers and the V_R/V_S value for EF5 were 93.90 ± 4.35 μmol h^{-1}, 79.99 ± 3.18 μmol h^{-1}, and 1.17, respectively, at 30°C as compared with values of 17.05 ± 1.24 μmol h^{-1}, 0.13 ± 0.01 μmol h^{-1}, and 131.15, respectively, at 5°C. These results demonstrated that the lower values of V_R/V_S at 30°C caused a lower *R*-enantioselectivity; therefore, it is critical to increase the *R*-enantioselectivity of the protein at the high-yield temperature of 30°C.

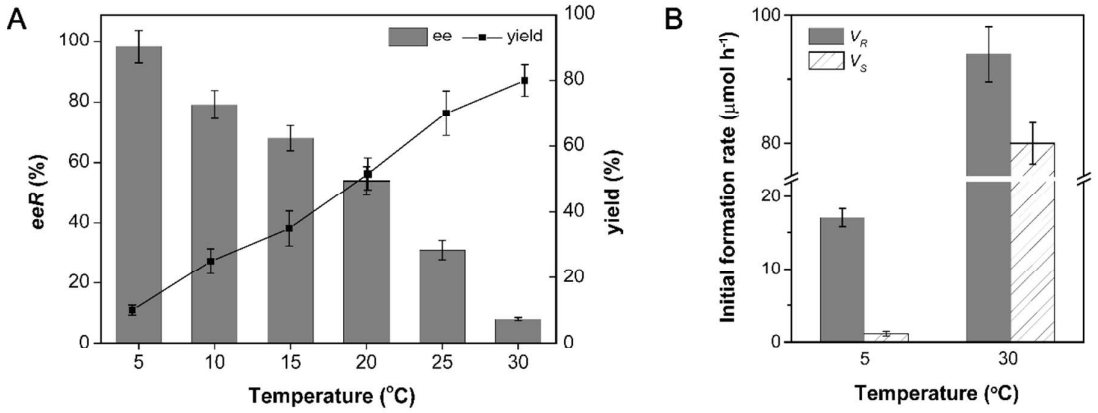

Figure 1. Effect of temperature on the enantioselectivity (A) and initial formation rate (B) of the EF5 mutant.

Engineering CALB Conformational Dynamics

To understand how temperature affects the initial formation rates of the *R*- and *S*-enantiomers and, therefore, the enantioselectivity, MD simulations were performed for the EF5 mutant at 5°C and 30°C on the basis of *R*- or *S*-enantiomer-bound structures. As shown in Figure 2, the root-mean-square fluctuations (RMSFs) of α-carbons were calculated to analyze changes in dynamics, resulting in increases in the RMSFs around regions 1, 2, and 3, the components of the CALB active pocket and channel, at 30°C as compared with those at 5°C. Combining the results of Figure 2 and Figure 1B, we deduced that high temperature led to an increase in the conformational dynamics of the active pocket and channel (Figure 2), which enhanced the catalytic rate of the *S*-enantiomer (Figure 1B), thereby decreasing the *R*-ee value. Therefore, modulating conformational dynamics around the CALB active pocket and channel provided a potential strategy for increasing *R*-enantioselectivity at 30°C.

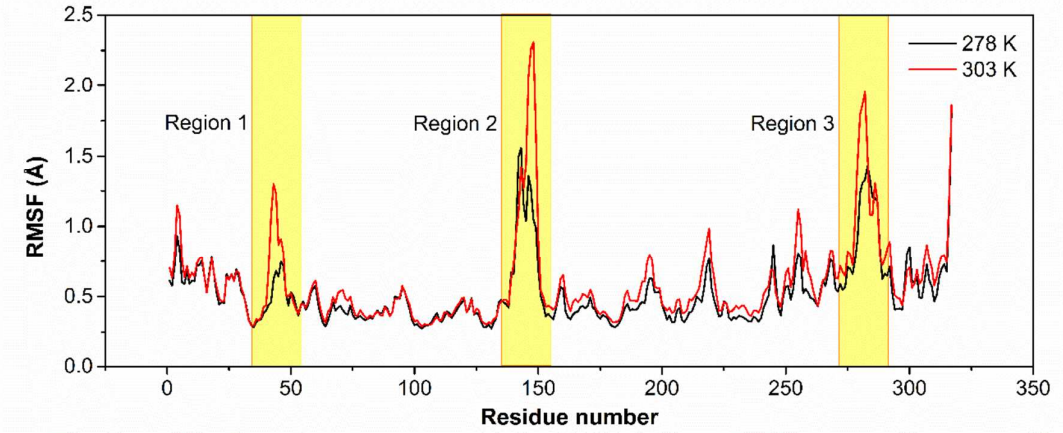

Figure 2. RMSFs calculated from MD simulations for the EF5 mutant at 5°C and 30°C.

We selected mutation candidates based on the analysis of the CALB active pocket (Figure 3)[29] and the following considerations: to avoid large alterations in main-chain dynamics and secondary structure distortion, candidate mutations were mainly inserted within the loop regions of the pocket, excluding proline and glycine.[22] We chose six residues (D134, A148, V149, I189, V190, and Q157) in region 2 (the acyl-binding pocket) and five residues (T42, T43, W104, A281, and A282) in regions 1 and 3 (the alcohol-binding pocket and channel). Furthermore, residues D223 and T186, which are adjacent to the catalytically active H224 and D187, respectively, and might affect enantioselectivity, were also selected.

Alanine scanning is an important method for protein engineering. Here, candidate residues (except for alanine) were computationally substituted with alanine, and MD simulations involving these mutations were performed at 30°C, with A281 and A282 were computationally substituted with serine, which exhibits a similar size and different properties than alanine. The results presented in Figure S1 showed that among the mutations, the RMSFs for D223A and A281S showed clear changes around regions 1 and 2 and regions 1 and 3, respectively. Therefore, residues D223 and A281 were identified for further mutational analyses.

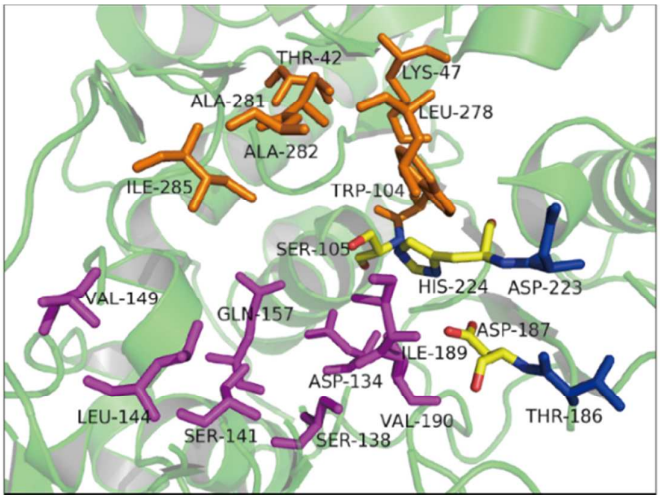

Figure 3. The CALB active pocket. CALB is traditionally considered as having two binding domains capable of harboring esters: one for the acid (acyl) moiety and the other for the alcohol moiety of the ester. Changes in pocket conformation might result in different substrate-binding modes, thereby showing different selectivity. The acyl- and alcohol-binding pockets are shown in purple and brown, respectively. D223 and T186 are shown in blue. The triad D187-H224-S105 lies between the two pockets. Residues A281, A282, and I285 point toward the alcohol moiety of the ligand and limit the size of the channel.

With the key residues D223 and A281 as candidates, these amino acids were subject to further mutation, resulting in 38 candidate mutants subsequently analyzed by MD simulation (Figure S6). Among these, the RMSFs of D223V and A281S were reduced around regions 1 and 2 and regions 1 and 3, respectively (Figure S2). Moreover, an MD simulation was also conducted for the double mutant D223V/A281S, with more obvious decreases in the RMSFs around regions 1, 2, and 3 observed as compared with those observed in the single mutants (Figure S3). In particular, the double mutant D223V/A281S exhibited the largest decrease in RMSF of nearly 1.1 Å around region 2 as compared with that in the EF5 mutant (ΔRMSF; Figure 4). Therefore, we selected D223V, A281S, and D223V/A281S as the optimal mutants expected to enhance enantioselectivity at 30°C by decreasing the conformational dynamics of the pocket and channel.

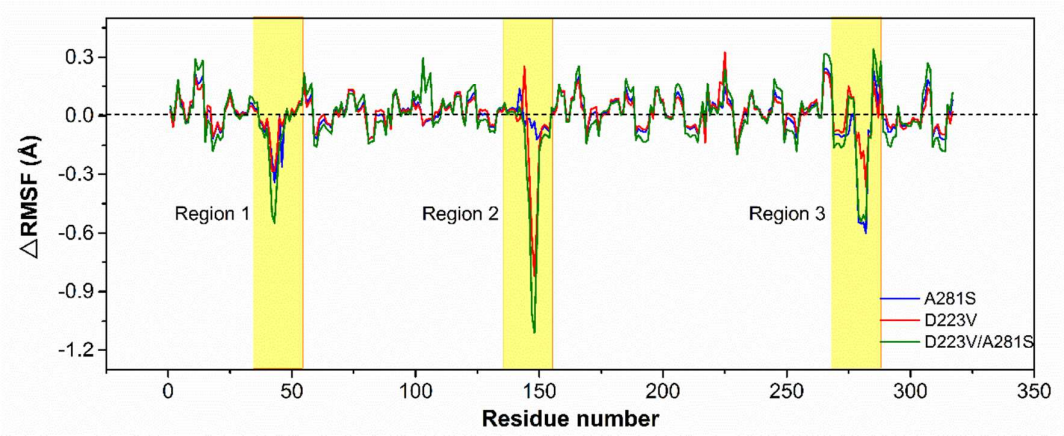

Figure 4. Differences in the RMSFs (ΔRMSF) of the mutants EF5 and A281S, D223V, and D223V/A281S.

Computational Evaluation of CALB Mutants

Changes in the pockets and channels of the selected CALB mutants (D223V, A281S, and D223V/A281S) were investigated using MD simulations under a constant temperature of 30°C (Figure 5). Compared with those of the EF5 mutant, the conformational dynamics of the pocket and channel of the D223V/A281S mutant were reduced, resulting in decreases in the hydrogen-bond distance between the main-chain amide of Q157 and the carboxyl group of the *R*-enantiomer from 5.70 Å to 3.00 Å and the distance between H224 (the HE2 atom) and S105 (the OG atom) from 2.60 Å to 2.30 Å (Figure 5A and B). These results clearly indicated that decreasing the conformational dynamics resulting in strengthening of the structural constraints of the pocket and channel.

Furthermore, we found that one important hydrogen bond between H224 and the oxygen of the

S-enantiomer was lost (Figure S7). Therefore, we compared the distances between H224 (the HE2 atom) and the oxygen (the O_2 atom) of the *R*-enantiomer (distance d_1) and the *S*-enantiomer (distance d_2), as well as the corresponding binding energies. As shown in Table S1, the CALB mutants (D223V, A281S, and D223V/A281S) exhibited decreases in d_1, increases in d_2, and larger differences in the binding energies of the *R*- and *S*-enantiomers as compared with those of the EF5 mutant. When compared with the corresponding values for the EF5 mutant (Figure 5), the d_1 value in the D223V/A281S mutant decreased from 3.50 Å to 2.60 Å, whereas the d_2 value increased from 3.80 Å to 4.30 Å. The distances separating the catalytic serine and the new ester O_2 of the *R*-enantiomer (distance d_3) and the *S*-enantiomer (distance d_4) showed similar changing trends as those of d_1 and d_2, respectively (Table S4). The binding energy to the *R*-enantiomer was –410.27 ± 9.30 kJ/mol, and that of the *S*-enantiomer was –392.78 ± 12.65 kJ/mol; therefore, the difference in the binding energies of the two enantiomers increased to 17.49 kJ/mol from 3.86 kJ/mol in the EF5 mutant. The oxyanion hole (Q106 and T40) plays an important role in stabilizing the transition state of the reaction. As shown in Figure S7, the *R*-enantiomer is favorably stabilized by formation of two hydrogen bonds with Q106 and T40, respectively, whereas this occurs in the *S*-enantiomer with only with T40. These results clearly indicated that decreasing conformational dynamics led to a strengthening of the structural constraints of the pocket and channel, which might represent the improvement in *R*-enantioselectivity.

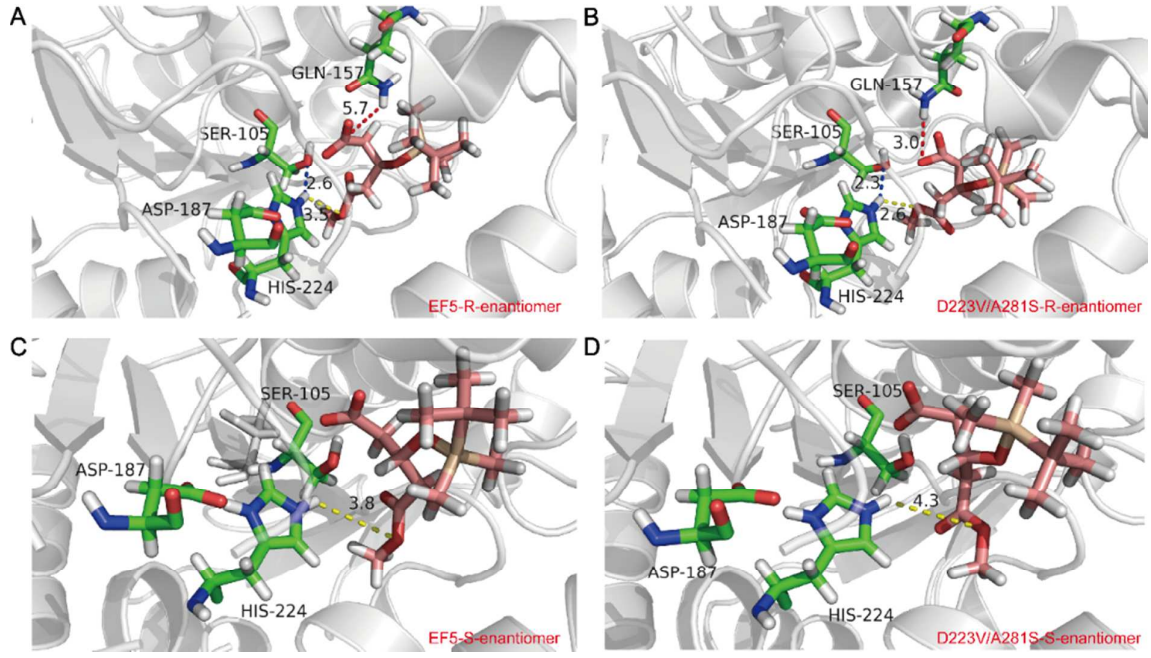

Figure 5. Comparison and analysis of differences between *R*/*S*-enantiomer-bound EF5 and D223V/A281S. (A) The *R*-enantiomer-EF5 complex, (B) the *R*-enantiomer-D223V/A281S complex, (C) the *S*-enantiomer-EF5 complex, and (D) the *S*-enantiomer-D223V/A281S complex. The hydrogen-bond distance between Q157 and the carboxyl group of the *R*-enantiomer is shown in red (A, B). The distance between H224 (the HE2 atom) and S105 (the OG atom) is shown in blue (A, B). The distances (d_1/d_2) between H224 (the HE2 atom) and the bound *R*/*S*-enantiomer oxygen (the O_2 atom) are shown in yellow (A–D).

Experimental Evaluation of CALB Mutants

The mutants D223V, A281S, and D223V/A281S were constructed through site-directed mutagenesis (Figure S4), and the initial formation rates of the *R*- and *S*-enantiomers of each mutant were detected at 30°C (Table 1). As illustrated in Table 1, the V_S values of the A281S, D223V, and D223V/A281S mutants significantly decreased from 79.99 ± 3.18 in the EF5 mutant to 3.14 ± 0.04, 2.00 ± 0.01, and 0.46 ± 0.01 μmol h^{-1}, respectively. However, compared with that of the EF5 mutant, the V_R values decreased only slightly (Table 1). Additionally, the V_R/V_S values increased from 1.17 (the EF5 mutant) to 29.78 (A281S), 46.71(D223V), and 200.11(D223V/A281S). Overall, we hypothesized that decreases in the dynamics of the pocket and channel resulting from mutations at sites 223 and 281 might lead to a sharp decline in the initial formation rate of the *S*-enantiomer, thereby increasing *R*-enantioselectivity at 30°C.

Table 1 The initial formation rates of *R*- and *S*-enantiomers catalyzed by CALB mutants at 30°C.

Mutants	Initial formation rate [μmol h^{-1}]		V_R/V_S
	V_R	V_S	
EF5	93.90 ± 4.35	79.99 ± 3.18	1.17
A281S	93.52 ± 8.02	3.14 ± 0.04	29.78
D223V	93.42 ± 2.35	2.00 ± 0.01	46.71
D223V/A281S	92.05 ± 4.82	0.46 ± 0.01	200.11

The kinetic parameters of the CALB mutants were determined using optically pure *R*- and *S*-enantiomers as substrates and compared, with the results are listed in Table 2. For the D223V/A281S mutant, the k_{cat}, K_M, and k_{cat}/K_M values toward the *R*-enantiomer were 5.60% higher, 34.00% lower, and 58.00% higher, respectively, than the corresponding values in the EF5 mutant. The k_{cat}, K_M, and k_{cat}/K_M values toward the *S*-enantiomer exhibited a 13.94% decrease, 30.86-fold increase, and 35.00-fold decrease, respectively, as compared with the corresponding values in the EF5 mutant. Furthermore, the esterification reactions (Scheme 1) catalyzed by the EF5, D223V, A281S, and D223V/A281S mutants were investigated at a 3-L scale at 30°C, with the results listed in

Table 3. The conversion yields of (*R*)-3-TBDMSO glutaric acid methyl monoester were >80.00% using the CALB mutants at 30°C, and for the D223V/A281S mutant, the *R*-ee value and the space-time yield were >99.00% and 107.54 g L^{-1} d^{-1}, respectively, at 30°C, whereas the *R*-ee value and the space-time yield of the EF5 mutant were 8.00% and 110.11 g L^{-1} d^{-1} at 30°C. As expected, the experimental results demonstrated that increased *R*-enantioselectivity was achieved with the D223V/A281S mutant at 30°C, consistent with results from MD simulations.

Table 2 Kinetic parameters of CALB mutants

Mutant	*R*-enantiomer				*S*-enantiomer			
	k_{cat} [s^{-1}]	K_M [mM]	k_{cat}/K_M [mM^{-1} s^{-1}]	Fold change	k_{cat} [s^{-1}]	K_M [mM]	k_{cat}/K_M [mM^{-1} s^{-1}]	Fold change
EF5	4.96 ± 0.24	0.60 ± 0.01	8.29	1.00	4.59 ± 0.15	0.64 ± 0.02	7.12	1.00
A281S	5.02 ± 0.33	0.43 ± 0.03	11.67	1.41	4.52 ± 0.39	11.59 ± 1.07	0.39	0.06
D223V	5.13 ± 0.36	0.42 ± 0.02	12.21	1.47	4.01 ± 0.12	15.42 ± 0.98	0.26	0.04
D223V/ A281S	5.24 ± 0.47	0.40 ± 0.04	13.10	1.58	3.95 ± 0.46	19.75 ± 3.81	0.20	0.03

Table 3 Production of *R*-enantiomers by CALB mutants

Mutants	Temperature [°C]	Time [h]	ee_R [%]	Conv. [%]	Space-time yield [$g \cdot L^{-1} \cdot d^{-1}$]
EF5	5	60	98.50	70.49	18.89
EF5	30	12	8.00	82.17	110.11
A281S	30	12	93.50	81.23	108.85
D223V	30	12	95.80	79.75	106.87
D223V/A281S	30	12	>99.00	80.25	107.54

CONCLUSIONS

In conclusion, the conformational dynamics of the CALB pocket and channel were engineered to successfully overcome the low enantioselectivity of the EF5 mutant at high temperatures toward (*R*)-3-TBDMSO glutaric acid methyl monoester and increase the ee value at 30°C. The most successful mutant, D223V/A281S, obtained following structural analysis and MD simulations showed a high *R*-ee value (>99.00%), explained by computational evaluation, and a high space-time yield (107.54 g L^{-1} d^{-1}). Mutations caused decreases in the conformational dynamics of the pocket, thereby enhancing enzyme enantioselectivity toward the *R*-form isomer, even at higher temperature. By contrast, a recent study showed that mutations increased the flexibility around the binding pocket

and induced higher activity in the thermophilic enzyme alcohol dehydrogenase at ambient temperature.[38] Although the design methods for mutants differed, these two studies both achieved changes in the flexibility of the active pocket by mutation, thereby adjusting the effect of temperature on enzyme properties. Our results lay the foundation for the industrialization of (*R*)-3-TBDMSO glutaric acid methyl monoester and provided insights for enzyme design guided by the engineering of conformational dynamics to solve issues related to enzymes exhibiting satisfactory enantioselectivity only at low temperatures and decreasing enantioselectivity at higher temperatures.

EXPERIMENTAL SECTION

Materials

The expression plasmid pGAPZαA was purchased from Novagen (Madison, WI, USA). The host strain *Pichia pastoris* GS115 was purchased from Invitrogen (Carlsbad, CA, USA). The restriction enzymes (*Xba*I, *Xho*I, *Dpn*I, and *AVr*II), T4 DNA ligase, primerSTAR polymerase, plasmid miniprep kit, and agarose gel DNA purification kit were supplied by TaKaRa (Dalian, China). The 3-TBDMSO glutaric anhydride was purchased from Henan Yuchen Fine Co., Ltd. (Henan, China). Hexane and isopropanol [high-performance liquid chromatography (HPLC)-grade] were purchased from Fisher Chemical (Fairlawn, NJ, USA). The (*R*)-3-TBDMSO glutaric acid methyl monoester standard and racemic 3-TBDMSO glutaric acid methyl monoester were gifted from Chanyoo Pharmatech Co., Ltd. (Nantong, China). A Daicel chiralpak AD-H column (4.6 × 250 mm) was purchased from Daicel Chiral Technologies Co., Ltd. (Shanghai, China). Other chemicals and solvents (analytical grade) were obtained from local suppliers.

Molecular Modeling and MD Simulations

The theoretical structures of CALB were downloaded from the Protein Data Bank (PDB: 1TCA), and structures of the mutants were obtained by homology modeling.[39] The three-dimensional structures of product enantiomers [(*R*)-1 and (*S*)-1] were obtained using the ChemOffice Ultra 11.0 program (CambridgeSoft; Perkin Elmer, Billerica, MA, USA). The tetrahedral intermediate, used as the transition state, was manually bound in the active site. Partial charges and force-field parameters for the substrates were automatically generated using the antechamber program using the general AMBER force field (http://ambermd.org/). Nonpolar hydrogen atoms were added to the enzyme

using the GROMACS 4.5.5 simulation package (http://www.gromacs.org/). The protonation state of residues was set according to pH 7.0. Na^+ counterions were added to neutralize the system, and the whole system was immersed in a cubic box of TIP3P water molecules, which was extended 10 Å from the dissolved atoms in all three dimensions. MD simulations were performed with GROMACS 4.5.5 and an AMBER03 force field following the three main steps of energy minimization, system equilibration, and production protocols.[40,41] Following steepest-descent energy minimization, 10-ns simulations were run at different temperatures in 2-fs steps. All simulations were performed individually for both (*R*)- or (*S*)-1-bound structures, and the binding energies and distances for hydrogen bonds were calculated. The enzyme and product were assigned to separate energy groups, and the binding energies between them were calculated as total inter-group potential energy.

Construction, Purification, and Immobilization of the CALB Mutants

Polymerase chain reactions (PCR) were performed using the EF5 plasmid (pGAPZαA-EF5) as a template and primers (Table S2). *Dpn*I (1 μL of 10 U μL^{-1}) was added to 25 μL of the PCR reaction mixture and incubated for 3 h at 37°C to eliminate the template plasmid. The digested product was transformed into *Escherichia coli* JM109 cells for amplification. Plasmid pGAPZαA mutants were obtained from *E. coli* JM109 cells, linearized by *Avr*II, purified, and transformed into *P. pastoris* GS115. *P. pastoris* GS115 was inoculated into yeast extract peptone dextrose medium (10 g L^{-1} yeast extract, 20 g L^{-1} peptone, and 20 g L^{-1} glucose) and grown at 30°C on a rotary shaker (200 rpm) for 2 days. The supernatant was harvested by aspiration and purified on a nickel-affinity column (Ni Sepharose 6 Fast Flow; Amersham Biosciences, Freiburg, Germany) to analyze the kinetic parameters.[42] Enzyme purity was tested by sodium dodecyl sulfate polyacrylamide gel electrophoresis (SDS-PAGE) (Figure S4). The supernatants of the mutants were mixed with D101 macroporous resin (Shanghai Hualing Resin Factory, Shanghai, China) for immobilization at 37°C for 5 h. The resin was filtered and dried under a vacuum, and the immobilized enzyme was used for esterification in the organic phase.

Measurement of the Initial Formation Rate of Each Enantiomer for Esterification

For the esterification (ring opening), 1.23 mM 3-TBDMSO glutaric anhydride and 1.23 mM methanol were dissolved in acetonitrile (5 mL), followed by ultrasonic dispersion and the addition of

enzyme (400 mg). The mixed system was shaken (200 rpm/min) at 5°C or 30°C, and at appropriate times, samples were analyzed by HPLC. Several data points were collected to determine the initial formation rate of each enantiomer. The activities of the immobilized mutant enzymes were maintained at the same level.

Measurement of the Kinetic Parameters of CALB Mutants

The kinetic parameters, including K_M and k_{cat}, of the *R/S*-enantiomers were calculated by measuring the initial rates of product formation at different concentrations of *R/S*-enantiomers (1–20 mM) at 30°C (ring forming). Samples were withdrawn, extracted, and analyzed by HPLC, and all assays were performed at least three times. The data were plotted, and K_M and k_{cat} values were obtained by the double reciprocal method.

Determination of the ee Values and Conversion Rates of CALB Mutants

The reaction (ring opening) was performed with immobilized EF5 and new mutants (80 g L^{-1}) in acetonitrile containing 60 g L^{-1} 3-TBDMSO glutaric anhydride with methanol for 12 h at different temperatures (5–30°C). The activity of each immobilized mutant enzyme was maintained at the same level. The concentrations of (*R*)-3-TBDMSO glutaric acid methyl monoester and the enantioselectivity were determined by HPLC using a mobile phase consisting of 96% hexane and 4% isopropanol with 0.02% (v/v) trifluoroacetic acid and filtered through a 0.22-μm membrane before use. Analysis (210 nm) was performed by injecting a 20-μL sample into the chromatograph, with a detection temperature of 25°C, a 1-mL/min flow rate, and a sample detection time of 15 min. The ee value was defined as follows: $ee_R = (R - S) / (R + S) \times 100\%$, where R and S represent the concentrations of the *R*- and *S*-enantiomers, respectively.

CONFLICTS OF INTEREST

The authors declare no competing financial interest.

FUNDING SOURCES

Financial support from the National Natural Science Foundation of China (21422602), the National Natural Science Foundation of China (21676118), the Special Foundation for State Key Research

and Development Program of China (2016YFD0400801), and Jiangsu Province "333 High-level Talents Cultivating Project" (BRA2016365) is gratefully acknowledged.

SUPPORTING INFORMATION

Supporting results, including details of RMSFs of the candidates (Figures S1–S3), SDS-PAGE of pure CALB mutants (Figure S4), chiral HPLC data of the esterification (Figure S5), details of RMSDs of the candidates (Figure S6), hydrogen-bond interaction data in D223V/A281S (Figure S7), hydrogen-bond distances and the binding energy of *R*- or *S*-tetrahedral intermediates in CALB mutants (Tables S1 and S4), primers used in this work (Table S2), information about mutant immobilization (Table S3).

REFERENCES

(1) Tan, Z.; Ma, H.; Li, Q.; Pu, L.; Cao, Y.; Qu, X.; Zhu, C.; Ying, H. *Enzyme Microb. Technol.* **2016**, *93*, 191-199.
(2) Qi, S.; Liu, C. Y.; Ding, J. Y.; Han, F. S. *Chem. Commun.* **2014**, *50*, 8605-8608.
(3) Bordeaux, M.; Tyagi, V.; Fasan, R. *Angew. Chem. Int. Ed.* **2015**, *54*, 1744-1748.
(4) Toda, H.; Ohuchi, T.; Imae, R.; Itoh, N. *Appl. Environ. Microbiol.* **2015**, *81*, 1919-1925.
(5) Shang, Y. P.; Chen, Q.; Kong, X. D.; Zhang, Y. J.; Xu, J. H.; Yu, H. L. *Adv. Synth. Catal.* **2017**, *359*, 426-431.
(6) Zheng, Y. C.; Xu, J. H.; Wang, H.; Lin, G. Q.; Hong, R.; Yu, H. L. *Adv. Synth. Catal.* **2017**, *359*, 1185–1193.
(7) Fillat, A.; Romea, P.; Urpí, F.; Pastor, F. I.; Diaz, P. *Appl. Microbiol. Biotechnol.* **2014**, *98*, 4479-4490.
(8) Sakai, T.; Kawabata, I.; Kishimoto, T.; Ema, T.; Utaka, M. *J. Org. Chem.* **1997**, *62*, 4906-4907.
(9) Sakai, T. *Cheminform* **2010**, *36*, 2749-2756.
(10) Liu, J. Y.; Zheng, G. W.; Imanaka, T.; Xu, J. H. *Biotechnol. Bioproc. E.* **2014**, *19*, 442-448.
(11) Sakai, T.; Kishimoto, T.; Tanaka, Y.; Ema, T.; Utaka, M. *Tetrahedron Lett.* **1998**, *39*, 7881-7884.
(12) Torres, R.; Ortiz, C.; Pessela, B. C.; Palomo, J. M.; Mateo, C.; Guisán, J. M.; Fernández-Lafuente, R. *Enzyme Microb. Technol.* **2006**, *39*, 167-171.
(13) Luetz, S.; Giver, L.; Lalonde, J. *Biotechnol. Bioeng.* **2008**, *101*, 647-653.
(14) Liu, J. Y.; Bian, H. P.; Tang, Y.; Bai, Y. P.; Xu, J. H. *Appl. Microbiol. Biotechnol.* **2015**, *99*, 1701-1708.
(15) Jiménez-Osés, G.; Osuna, S.; Gao, X.; Sawaya, M. R.; Gilson, L.; Collier, S. J.; Huisman, G. W.; Yeates, T. O.; Tang, Y.; Houk, K. *Nat. Chem. Biol.* **2014**, *10*, 431-436.
(16) Palmer, A. G. *J. Magn. Reson.* **2014**, *241*, 3-17.
(17) Boehr, D. D.; Nussinov, R.; Wright, P. E. *Nat. Chem. Biol.* **2009**, *5*, 789-796.
(18) Goodey, N. M.; Benkovic, S. J. *Nat. Chem. Biol.* **2008**, *4*, 474-482.
(19) Boehr, D. D.; Dyson, H. J.; Wright, P. E. *Chem. Rev.* **2006**, *106*, 3055-3079.
(20) Raza, S.; Fransson, L.; Hult, K. *Protein Sci.* **2001**, *10*, 329-338.
(21) Seo, M. H.; Park, J.; Kim, E.; Hohng, S.; Kim, H. S. *Nat. Commun.* **2014**, *5*, 3724-3730.
(22) Han, S. S.; Kyeong, H. H.; Choi, J. M.; Sohn, Y. K.; Lee, J. H.; Kim, H. S. *ACS Catal.* **2016**, *6*, 8440-8445.
(23) Hu, Y.; Liu, H. *J. Phys. Chem. A* **2014**, *118*, 9272-9279.
(24) Nichols, S. E.; Swift, R. V.; Amaro, R. E. *Curr. Top. Med. Chem.* **2012**, *12*, 2002-2012.

(25) Tiwari, M. K.; Singh, R.; Singh, R. K.; Kim, I.-W.; Lee, J.-K. *Comput. Struct. Biotechnol. J.* **2012**, *2*, 1-13.
(26) Parigi, G.; Rezaei-Ghaleh, N.; Giachetti, A.; Becker, S.; Fernandez, C.; Blackledge, M.; Griesinger, C.; Zweckstetter, M.; Luchinat, C. *J. Am. Chem. Soc.* **2014**, *136*, 16201-16209.
(27) Teague, S. J. *Nat. Rev. Drug. Discov.* **2003**, *2*, 527-541.
(28) Park, A.; Kim, S.; Park, J.; Joe, S.; Min, B.; Oh, J.; Song, J.; Park, S.; Park, S.; Lee, H. *ACS Catal.* **2016**, *6*, 7458-7465.
(29) Wu, Q.; Soni, P.; Reetz, M. T. *J. Am. Chem. Soc.* **2013**, *135*, 1872-1881.
(30) Sharma, D.; Sharma, B.; Shukla, A. *Biotechnology* **2011**, *10*, 23-40.
(31) Baldessari, A. *Methods Mol. Biol.* **2012**, *861*, 445-456.
(32) Andualema, B.; Gessesse, A. *Biotechnology* **2012**, *11*, 100-118.
(33) Jaeger, K.; Dijkstra, B.; Reetz, M. *Annu. Rev. Microbiol.* **1999**, *53*, 315-351.
(34) Takwa, M.; Larsen, M. W.; Hult, K.; Martinelle, M. *Chem. Commun.* **2011**, *47*, 7392-7394.
(35) Xia, B.; Xu, J.; Xiang, Z. W.; Cen, Y. X.; Hu, Y. J.; Lin, X. F.; Wu, Q. *ACS Catal.* **2017**, *7*, 4542-4549.
(36) Wang, H.; Li, Z.; Yu, X.; Chen, R.; Chen, X.; Liu, L. *RSC Adv.* **2015**, *5*, 75160-75166.
(37) Wu, J.; Wang, H.; Yang, B.; Song, W.; Liang, C.; Liu, L. *RSC Adv.* **2017**, *7*, 38264-38272.
(38) Li, G.; Maria-Solano, M. A.; Romero-Rivera, A.; Osuna, S.; Reetz, M. T. *Chem. Commun.* **2017**, *53*, 9454-9457.
(39) Biasini, M.; Bienert, S.; Waterhouse, A.; Arnold, K.; Studer, G.; Schmidt, T.; Kiefer, F.; Cassarino, T. G.; Bertoni, M.; Bordoli, L. *Nucleic Acids Res.* **2014**, *42*, W252-W258.
(40) Schmid, N.; Eichenberger, A. P.; Choutko, A.; Riniker, S.; Winger, M.; Mark, A. E.; van Gunsteren, W. F. *Eur. Biophys. J.* **2011**, *40*, 843-856.
(41) Van Der Spoel, D.; Lindahl, E.; Hess, B.; Groenhof, G.; Mark, A. E.; Berendsen, H. J. *J. Comput. Chem.* **2005**, *26*, 1701-1718.
(42) Li, X. J.; Zheng, R. C.; Ma, H. Y.; Zheng, Y. G. *Appl. Microbiol. Biotechnol.* **2014**, *98*, 2473-2483.

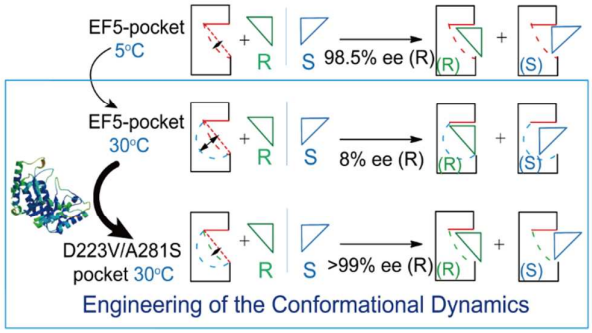

Table of Contents graphic